Microfluid Nanofluid
DOI 10.1007/s10404-010-0715-z

RESEARCH PAPER

Analysis of *mixed* motion in deterministic ratchets via experiment and particle simulation

T. Kulrattanarak · R. G. M. van der Sman · C. G. P. H. Schroën · R. M. Boom

Received: 13 April 2010 / Accepted: 9 June 2010

Abstract Deterministic lateral displacement (DLD) ratchets are microfluidic devices, which are used for size-based sorting of cells or DNA. Based on their size, particles are showing different kinds of motion, leading to their fractionation. In earlier studies, so-called zigzag and displacement motions are observed, and in recent study by our group (Kulrattanarak et al., Meas Sci Technol, 2010a; J Colloid Interface Sci, 2010b), we have shown that also *mixed* motion occurs, which is an irregular alternation of zigzag and displacement motion. We have shown that the mixed motion is due to asymmetry of the flow lane distribution, induced by the symmetry breaking of the oblique primitive lattice cell (Kulrattanarak et al. 2010b). In this study, we investigate *mixed* motion in depth by numerical and experimental analysis. Via 3D simulations, we have computed explicit particle trajectories in DLD, and are able to show that there are two critical length scales determining the type of motion. The first length scale $d_{f,1}$ is the first flow lane width, which determines the transition between zigzag motion and mixed motion. The other length scale, $d_{f,c}$, determines the transition between mixed motion and displacement motion. Based on our experimental and numerical results we have been able to correlate the migration angle of particles showing mixed motion to the particle size, relative to the two critical length scales $d_{f,1}$ and $d_{f,c}$.

Keywords Deterministic ratchet · Fractionation · Numerical simulation · Mixed motion

T. Kulrattanarak · R. G. M. van der Sman (✉) · C. G. P. H. Schroën · R. M. Boom
Food Process Engineering Group, Wageningen University, P.O. Box 8129, 6700 EV Wageningen, The Netherlands
e-mail: Ruud.vandersman@wur.nl

1 Introduction

Deterministic ratchets, also known as deterministic lateral displacement (DLD) arrays, are microfluidic devices used for size-based fractionation of suspensions. Although these ratchets are mainly investigated in biological applications, e.g., cells, DNA, and blood (Huang et al. 2004; Inglis et al. 2006; Davis et al. 2006; Loutherback et al. 2009; Green et al. 2009; Inglis et al. 2010; Loutherback et al. 2010; Al-Fandi et al. 2010), they also have potential for large-scale fractionation of food suspensions (Kulrattanarak et al. 2008).

Nowadays, fractionation of food materials receives much interest since it is expected to lead to more sustainable and economical use of agrifood materials, leading to multiple functional ingredients. Membranes have been considered for fractionation of food suspensions (Kromkamp et al. 2006a; Brans et al. 2007), but especially the larger components were found to influence the fractionation process negatively via membrane fouling. As an alternative technique, we have considered microfluidic devices, and found that DLD (deterministic lateral displacement) ratchets are the most promising option (Kulrattanarak et al. 2008). The main benefit of DLD ratchets over membranes is that they have much lower chance of particle blockage, as their characteristic dimension is larger than all particles, where in membranes the pores are smaller than the largest particle. Application of DLD ratchets for food applications can be more demanding than for biological applications, as food industry is interested in fractionation of concentrated suspensions, and at high throughput.

The fractionation principle of deterministic (DLD) ratchets is based on the flow line sieving principle (Eijkel and van den Berg 2006). When particles are large enough, hydrodynamic and steric interaction with regularly arranged obstacles can make them deviate from their original

Published online: 24 October 2010

streamline, via which they can end up in a different outlet than smaller-sized particles. In deterministic ratchets, one uses the interaction of the particles with an array of obstacles. A periodic cell of such an array is shown in Fig. 1. The space between two obstacles in a single row is subdivided into a number of flow lanes, which are separated by dividing streamlines. These dividing streamlines originate from the back of the obstacle, and end at the stagnation point at the front of an obstacle directly upstream. Each flow lane can be characterized by its width, $d_{f,i}$, between obstacles.

Particles larger than the first lane width, $d_{f,1}$, will have hydrodynamic/steric interaction with the obstacles, which makes them cross the dividing streamline, and they will end up in the adjacent flow lane. An important characteristic of the deterministic ratchet is that subsequent obstacle rows are displaced a fraction, $\Delta\lambda$, of the obstacle interspacing λ. Hence, particles which have crossed the dividing streamline via interaction with an obstacle will bump onto the obstacle of the following row (*displacement* motion). Inglis et al. (2006) have noted that particles larger than $d_{f,1}$ will move along in the lattice direction under angle $\theta_{\max}$ relative to the flow direction, as shown in Fig. 1.

The flow lane distribution is determined by the various geometrical parameters of the obstacle array, as displayed in Fig. 1, which comprise: R_o is the radius of obstacle, D_x is the gap width between the obstacles in flow direction, and D_y is the gap width perpendicular to the flow. The shift of the obstacle rows, $\Delta\lambda$, is a fraction of the distance between the centers of the obstacles denoted as $\lambda = D_y + 2R_o$. The ratio of $N = \lambda/\Delta\lambda$ is an integer, and indicates the number of obstacle rows in one periodic cell.

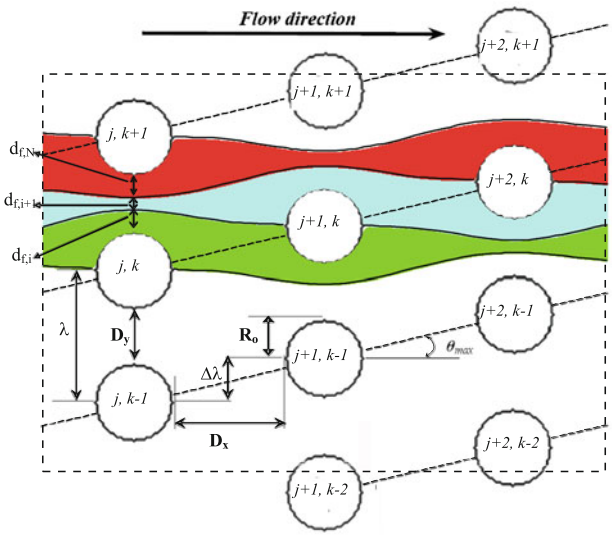

Fig. 1 A periodic cell with $N = 3$ obstacle rows. Various geometrical parameters are indicated with their symbols and measures. The space between obstacles in an obstacle row is subdivided into N flow lanes, each indicated by a *different color*. Flow lanes are characterized by its width $d_{f,i}$. The bounding (*solid*) lines of the flow lanes are dividing streamlines, originating and ending at stagnation point at the surface of the obstacles. *Dashed lines* indicate the migration angle $\theta_{\max}$ of particles showing displacement motion, and are the boundaries of the displacement lanes, within which the displacing particles move

Initially, Inglis et al. (2006) have assumed that between the obstacles a parabolic flow profile existed, with all flow lanes having equal volumetric flow rate. Consequently, the flow lane width distribution is non-uniform, with the first and the last flow lanes being equal and largest in size ($d_{f,1} = d_{f,N}$). Inglis et al. have stated that the first flow lane width is the critical length scale determining the transition between zigzag and displacement motion. Hence, particles with radius $r_p > d_{f,1}$ will show displacement motion, and zigzag motion otherwise.

From 2-D flow field simulations (Kulrattanarak et al. 2010b), we have found that for a large class of ratchet designs, with the interspacing ratio $D_x/D_y \leq 3$ and dimensionless obstacle radius $R_o/D_y > 0.2$, the flow lane width distribution is *asymmetric*, with the first lane width, smaller than the last one, $d_{f,1} < d_{f,N}$. For these devices we have found a new type of particle behavior for the medium-sized particles, which we have named *mixed* motion (Kulrattanarak et al. 2010a). The particles with mixed motion have migration angles θ in between those for zigzag ($\theta = 0$) and displacement motion ($\theta = \theta_{\max}$). Examples of these three types of particle motions are shown in Fig. 2. Here, one can clearly observe that the *mixed* motion is an alternating zigzag and displacement motion.

We have formulated the hypothesis that the asymmetry of the flow lane distribution introduces a second critical length scale, $d_{f,c}$ determining the transition between mixed motion and displacement motion (Kulrattanarak et al. 2010b). The first critical lengthscale, i.e., the width of the first flow lane $d_{f,1}$ determines the transition between zigzag and mixed motion. However, neither the 2D flow field simulations nor our previous experiments have given indications what precisely determines the second critical length scale, $d_{f,c}$. It appears that the degree of asymmetry, quantified as the ratio of the last to the first flow lane width $A = d_{f,N}/d_{f,1}$, is one of the main determining factors, but is moderated by additional factors like the design parameters D_x/D_y and R_o/D_y. The cause of the asymmetry in the flow lane width distribution is the symmetry breaking by the oblique primitive lattice cell, leading to anisotropy in the permeability of the obstacle array. Another way of inducing asymmetry in the flow lane distribution is asymmetry in the obstacle shape (Loutherback et al. 2009, 2010). Designing ratchets for the demanding food applications requires detailed knowledge on the determinants of $d_{f,c}$, what is pursued in this article.

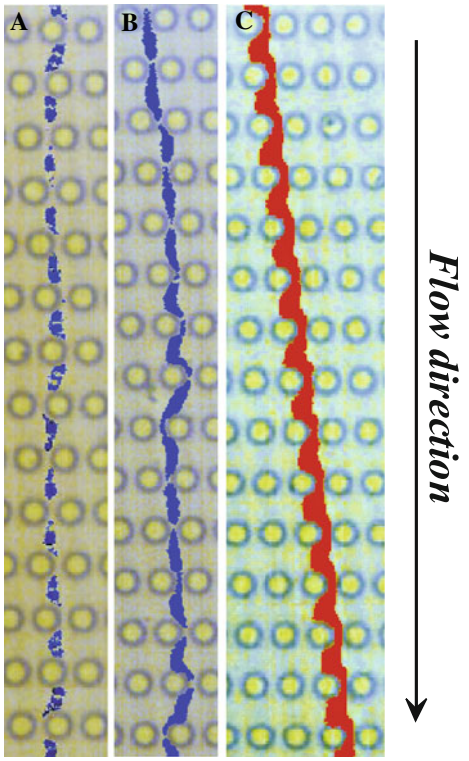

Fig. 2 Types of particle motion in deterministic ratchets: **a** zigzag motion, **b** mixed motion, and (**c**) displacement motion. Particles trajectories are obtained via image analysis in devices as described in Kulrattanarak et al. (2010a)

We investigate the validity of our hypothesis concerning mixed motion with further experiments and 3D simulations in which suspended particles are explicitly taken into account, which cannot be done through 2D simulations. We note that 3D particle simulations are scarcely performed for deterministic ratchets. We are aware of only one earlier study, by Frechette and Drazer (2009), who have performed Stokesian dynamics on a sphere sedimenting through a DLD ratchet, with a square primitive cell. We apply the Lattice Boltzmann method (Chen and Doolen 1998; Ladd and Verberg 2001), computing trajectories of spheres in pressure-driven flow through DLD ratchets, having an oblique primitive lattice cell, which is required to obtain an asymmetric flow lane distribution, and consequently mixed motion (Kulrattanarak et al. 2010b).

With our 3D particle simulations we compute the motion of a single particle through a periodic cell of a DLD device, having the same dimensionless design parameters (N, D_x/D_y, R_o/D_y) as the devices used in our experiments. These devices are especially designed for observation of mixed motion. From the 3D particle simulations we determine the second critical length scale $d_{f,c}$ via investigating at which particle size the transition to displacement motion occurs. From 2D simulations of the flow field in the new ratchet designs, we obtain the flow lane distribution, and thus also the first critical length $d_{f,1}$. These two critical length scales will be compared to the type of motions shown by particles in the newly designed ratchet devices. Via this comparison of simulation and experimental results, we formulate a correlation between the migration angle and the particle size, as compared to the two critical length scales $d_{f,1}$ and $d_{f,c}$.

2 Material and methods

2.1 Deterministic ratchet devices

We have designed deterministic ratchet devices that allow observation of mixed motion, based on the size distributions of the particle suspensions, and the asymmetry of the flow lane distribution. The designs are made such that one part of the particles suspensions is expected to show zigzag motion, and other part of the particle suspensions is expected to show mixed motion. The resulting designs are listed in Table 1. They are described in terms of dimensionless design parameters the number of rows in a periodic cell N, the ratio of the interspacings D_x/D_y, and the dimensionless obstacle radius R_o/D_y.

The ratchet devices are produced by Delft Institute of Microelectronics and Submicrontechnology (DIMES), affiliated with Delft University of Technology, the Netherlands. Using lithography and highly anisotropic DRIE processes, the cylindrical obstacles are etched in silicon, as described by Pham et al. (2009). For all these designs, it is observed that the height of the obstacles is 40 μm, the radius is in the range of $1.6 \lesssim R_o \lesssim 4$ μm, and the space between the obstacles is in the range , $8 \leq D_y \leq 9$ μm.

Each ratchet device has a chip size of 15 × 15 mm with 2 inlets, one for the particle suspensions and another one for the carrier fluid. All inlets and outlets have the same width, which is taken equal to the width of 3 periodic cells ($L_y/\lambda = 3N$). The length of the devices is taken such that if particles would show displacement motion they would end up in the outlet, and hence its length is $L_x/\lambda = 3N \times N$.

Table 1 Geometry of the devices and the first ($2d_{f,1}/D_y$) and the last flow lane widths ($2d_{f,N}/D_y$) determined from 2D-simulation (Kulrattanarak et al. 2010b)

Design	N	D_x/D_y	R_o/D_y	$2d_{f,1}/D_y$	$2d_{f,N}/D_y$
I	4	1.5	0.5	0.59	0.74
II		1.5	0.2	0.59	0.66
III	6	1.5	0.2	0.46	0.51
IV		2.0	0.2	0.47	0.48

2.2 Experimental setup

The latex suspensions are obtained from Interfacial Dynamics Corporation (USA), and have different nominal diameters, namely, 3.4, 4.0, 5.0, or 6.0 μm. The actual size distribution has been measured using dynamic light scattering with Malvern Mastersizer 2000 (Kulrattanarak et al. 2010a). The stock suspensions are diluted with MilliQ water to a volume concentration of 0.05%.

The ratchet devices are placed in a module (Fluidic connect 4515) from Micronit microfluidics B.V., the Netherlands. PEEK tubes with an internal diameter of 150 μm are used to connect the chip to syringes (1000 μL, Hamilton) placed in syringe-pumps (Harvard Apparatus model 11 plus) set at constant flow rates of 4 μL/h. One inlet is fed with the particle suspension, and the other outlet is fed with MilliQ water, the carrier fluid.

During the start-up of the experiment, 0.25 wt% Synperonic PEF108 solution is first pumped into the device to drive out air bubbles and pre-treat the surface of the device to prevent particle adhesion (Steegmans et al. 2009). After all bubbles are eliminated, we pump the solution through the chip for 30 min, after which we switch to particle suspensions.

The motion of particles through the ratchet devices is observed with a Zeiss Axioplan microscope, equipped with a Motion Pro high-speed camera (Redlake MASD Inc., San Diego). Video images are directly stored on the hard disk of a computer, which operates the camera using MIDAS software. Depending on the size and the speed of the particle and required quality of the video, we have used a magnification of 20–200, and a frame rate of 200–300 frames/s. The resolution of a video image can vary from 128 × 48 up to 1280 × 1024 pixels.

From the video images, particle trajectories are extracted with a sophisticated image analysis algorithm, which we have described in detail in our previous study (Kulrattanarak et al. 2010a). The algorithm is implemented in MATLAB software using the Image Processing Toolbox. From the particle trajectories, we can obtain the migration angle, which describes the direction of the particle trajectory with respect to the flow direction (Kulrattanarak et al. 2010a).

2.3 *2D* flow field simulations

The flow lane width distribution of the new ratchet designs is computed with the 2D flow simulation model described in our article (Kulrattanarak et al. 2010b). We have simulated the fluid flow through a periodic cell of various ratchet designs using the Lattice Boltzmann (LB) method, based on the generally applied Lattice BGK scheme, and specifically the two-dimensional D2Q9 scheme (Chen and Doolen 1998; Qian et al. 1992). The no-slip boundary condition at the interface of fluid and obstacles is implemented using the bounce-back method, as discussed in the review of Ladd and Verberg (2001). The pressure drop over the periodic cell is implemented using the "pressure periodic" boundary conditions as proposed by Inamuro et al. (1995). The Lattice Boltzmann code has been validated against a benchmark problem of Sangani and Acrivos (1982).

From the LB simulations, we obtain the steady state velocity field $\mathbf{u}(\mathbf{x})$ throughout the periodic cell of the ratchet. From the flow field we determine the sizes of the flow lanes via determining the trajectories of tracer particles. The particle trajectories are computing using the equation of motion, $\mathrm{d}\mathbf{x}/\mathrm{d}t = \mathbf{u}(\mathbf{x})$, integrated with the Euler forward method.

The width of flow lanes, $d_{f,i}$, is determined by releasing tracer particles at equidistant locations in the space between obstacles j, k and j, $k+1$ (see Fig. 1) in which j identifies the obstacle row number and k identifies the bounding line of a displacement lane. The tracer particle will perform a zigzag motion. How the tracer particles zigzags around the obstacles determines in which flow lane they are released, and the flow lane distribution is obtained. More details one finds in our previous article (Kulrattanarak et al. 2010b).

2.4 *3D* numerical simulations

The motion of spherical particles through a ratchet device is simulated with a three-dimensional Lattice Boltzmann code, which performs Direct Numerical Simulation (DNS) of a sphere in a flowing fluid. In DNS the sphere is fully resolved, meaning that the particle diameter is larger than the grid spacing $d_\mathrm{p} \gg \Delta x$ (van der Sman 2009). In DNS simulation, only few assumptions have to be made, and in this particular case, the only assumption is the form of the lubrication force between sphere and cylindrical obstacles if the gap between them is smaller than the grid spacing, $h < \Delta x$.

The particular Lattice Boltzmann method we have used is the Two-Relaxation-Time (TRT) scheme. The TRT scheme has been developed by Ginzburg (2005), and is an efficient implementation of the Multi-Relaxation-Time (MRT) scheme (d'Humieres et al. 2002). MRT schemes are known to eliminate the viscosity-dependent error in the effective radius of suspended particles and obstacles immersed in the flow. Via careful tuning of the degrees of freedom (DOF) of the TRT scheme, the error in the effective radius can be reduced significantly (Ginzburg 2005; Chun and Ladd 2007; van der Sman 2010a). For implementing the no-slip boundary conditions on the moving sphere, obstacles and confining microchannel, we have used the traditional bounce-back method, as originally

developed by Ladd (1994). Chun and Ladd (2007) have stated recently that the bounce-back method in combination with the TRT scheme is a very viable choice for implementing DNS simulations of suspensions with Lattice Boltzmann, in terms of accuracy, efficiency, and ease of implementation, what we have evidently shown in a recent article (van der Sman 2010a). From the analysis in that article, it is observed that the optimal value of the DOF should adhere to the following heuristic:

$$\left(\frac{1}{\omega^+}-\frac{1}{2}\right)\left(\frac{1}{\omega^-}-\frac{1}{2}\right)=\frac{1}{4} \quad (1)$$

with $\lambda^+ = 1 - \omega^+$ and $\lambda^- = 1 - \omega^-$ the eigenvalues of the Lattice Boltzmann collision operator, for respectively the even and odd non-hydrodynamic modes (van der Sman 2010a; Ginzburg 2005). λ^- is related to the viscosity of the fluid, via $\nu_f = c_s^2(\frac{1}{\omega^-}-\frac{1}{2})\Delta t$, with $c_s^2 = \frac{1}{3}(\Delta x/\Delta t)^2$ the speed of sound squared. λ^+ is not related to any physical property of the fluid and renders a DOF to minimize the error in the effective radius of the suspended sphere. In our earlier article (van der Sman 2010a), the accuracy of the TRT scheme was extensively benchmarked; therefore, we will use the method as such.

For the lubrication force between the moving sphere and the cylindrical obstacles at small distances, we use the hypothesis of Adamczyk et al. (1983)—likewise a recent article on deterministic ratchet devices by Frechette and Drazer (2009). Adamczyk states that the hydrodynamic interaction (lubrication force) between an unconfined sphere of radius a approaching a cylinder of radius R is equal to the hydrodynamic interaction between that particular sphere, with radius $r_{p,1} = a$, and a second, immobile sphere of a radius twice as large as that of the cylinder, i.e., $r_{p,2} = 2R$. We have tested the hypothesis of Adamczyk and found that it is valid at short distances $h/r_p \ll 1$. For distances further away the effect of the confining walls become noticeable—but this effect is sufficiently covered by the Lattice Boltzmann TRT scheme (van der Sman 2010b).

In summary, if the gap between sphere and cylindrical obstacle is less than one grid spacing, an explicit lubrication force acts on the particle—which is added to the force exerted on the particle by the fluid, as computed via the imposition of the no-slip boundary condition on the particle. As is stated in the original work of Ladd (1994), the explicit lubrication force is truncated beyond a certain cutoff length—which is here taken equal to the grid spacing Δx. Hence, if $h \geq \Delta x$ the lubrication force is zero.

The lubrication force scales with r_p/h, and diverges if the gap goes to zero, $h \to 0$, which is physically unrealistic (van der Sman 2009). A common practice is to let lubrication force saturate beyond a certain length scale, which can be interpreted as the particle roughness (Ball and Melrose 1995; Kromkamp et al. 2006b; van der Sman 2009). Here we take as the limiting length scale $h_{min} = 0.05\ r_p$. Furthermore, following Ball and Melrose (1995), we assume a Hookean spring force to act on the particle if $h < h_{min}$, which is linear with $h - h_{min}$. A sufficiently stiff spring will prevent the gap to become significantly smaller than h_{min}.

Simulations are performed for one single periodic cell of a deterministic ratchet. The fluid flow will be driven via a pressure gradient over the periodic cell. This pressure gradient can be imposed via pressure periodic boundary conditions along the flow direction, as follows from the scheme of Inamuro et al. (1995).

Also, for the suspended sphere we assume periodic boundary conditions in the flow direction. If the particle is crossing the pressure periodic boundary, the computation of the force imposed by the fluid on the particle has to account for the fact that there is a jump in the pressure between inlet and outlet. The initial position of the particle is midway the first and second row of obstacles, in front of a gap between two obstacles, and it is positioned midway the confining walls of the microchannel. Initially the fluid is at rest, and starts flowing due to the applied pressure gradient. To eliminate start-up effects in the particle trajectory, we allow the particle to traverse the periodic cell more than once; a particle which leaves the computational domain will enter the domain again at the opposite side.

At the confining walls of the microchannel, of height H, we impose no-slip boundary conditions using the half-way bounce-back method (Chun and Ladd 2007; van der Sman 2010a). As mentioned, at the remaining boundaries of the computation domain, we use regular periodic boundary conditions for both the fluid flow as for the suspended spheres.

3 Results and discussion

3.1 Comparison 3D-simulation with 2D-simulation

Via the 3D simulations we have computed the trajectories of particles traversing the periodic cell of the ratchet designs, which are listed in Table 1. Particle sizes are in the range of $2d_{f,1} \lesssim d_p < D_y$—with $d_{f,1}$ computed by the 2D flow simulations. In Figs. 3 and 4, we show the results for designs II and III, which are also illustrative for other devices. In these figures, we indicate the trajectories of particles (3D simulation) and superimposed them on the flow lanes, which are computed with 2D flow simulations.

The particle trajectories converge to a periodic motion, after they traverse once or twice the periodic cell. Remarkably, this limiting periodic motion is independent

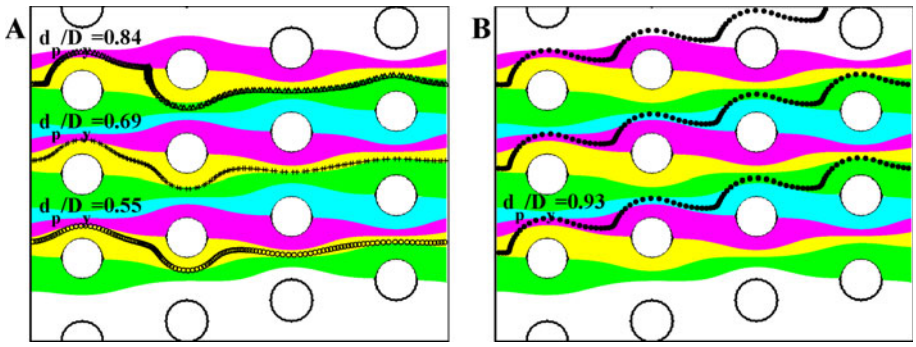

Fig. 3 Particle motion after the first cycle obtained via 3D-simulation of explicit particles in fluid flow through a periodic cell of ratchets with $N = 4$, $R_o/D_y = 0.5$, and $D_x/D_y = 1.5$ with **a** $d_p/D_y = 0.55$, 0.69 and 0.84, **b** $d_p/D_y = 0.93$ superimposed on the flow lanes obtained from 2-D flow field simulation giving $2d_{f,1}/D_y = 0.59$ and $2d_{f,N}/D_y = 0.74$. Flow lanes are given in different colors

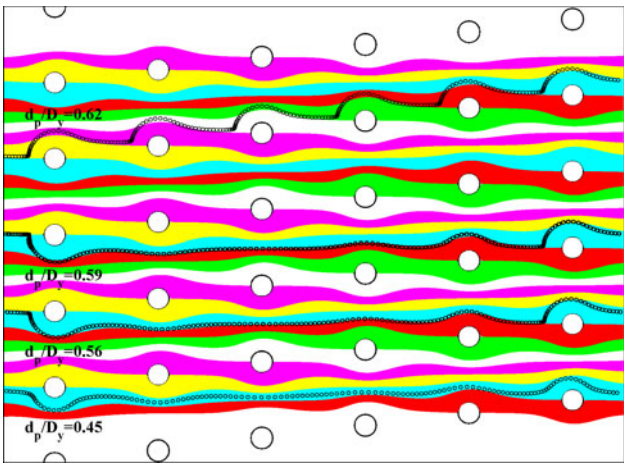

Fig. 4 Particle motion after the first cycle obtained via 3D-simulation of explicit particles in fluid flow through a periodic cell of ratchets with $N = 6$, $R_o/D_y = 0.2$, and $D_x/D_y = 1.5$ with $d_p/D_y = 0.45$, 0.56, 0.59 and 0.62 superimposed on the flow lanes obtained from 2-D flow field simulation giving $2d_{f,1}/D_y = 0.46$ and $2d_{f,N}/D_y = 0.51$. Flow lanes are given in *different colors*

Table 2 The critical length scales for the investigated devices, (1) $d_{f,I}$ obtained from (Inglis et al. 2006), (2) $2d_{f,1}/D_y$ and $2d_{f,N}/D_y$, obtained from 2D-simulation, and (3) the critical length scale $2d_{f,c}/D_y$ obtained from the 3D particle simulations

N	D_x/D_y	R_o/D_y	$2\ d_{f,I}/D_y$	$2d_{f,1}/D_y$	$2d_{f,N}/D_y$	$2d_{f,c}/D_y$
4	1.5	0.5	0.65	0.59	0.74	0.93
	1.5	0.2	0.65	0.59	0.66	0.86
6	1.5	0.2	0.52	0.46	0.51	0.62
	2.0	0.2	0.52	0.47	0.48	0.78

of the initial position of the particle, as we concluded from several simulations where we only changed the initial position (results not shows). Similar periodic trajectories being independent of initial position are also observed by Frechette and Drazer (2009) using simulations with Stokesian Dynamics.

The 3D simulations confirm that particles show zigzag motion, if their radius is smaller than the first flow lane width, $d_p < 2d_{f,1}$. In both Figs. 3a and 4, one can observe that these particles remain within their flow lanes. As shown in Fig. 3b, we observe that large particles exhibit displacement motion. They continuously bump into the obstacles, and move along the lattice direction having an angle of θ_{max} with the flow direction. The particle size for which we have found the transition to displacement motion determines the second critical length scale $d_p = 2\ d_{f,c}$. In Table 2 we have listed this critical length scale for all investigated ratchet designs. The second critical length scale does not appear not to be correlated with the last flow lane width $d_{f,N}$ or the first critical length scale $d_{f,1}$. However, for all designs, it is observed that $d_{f,c} > d_{f,N}$.

For particles with an intermediate size, $2d_{f,1} < d_p < 2d_{f,c}$, the 3D simulations show a different type of motion, but it is different from the experimentally observed mixed motion (Kulrattanarak et al. 2010a). During the hydrodynamic interaction with the obstacles, the intermediate sized particles are crossing the bounding streamline of the first flow lane. However, they do that twice, and subsequently they follow this dividing streamline until they approach the stagnation point of the obstacle, where the dividing streamline terminates. During this approach the particles are slowed down significantly due to the (dissipative) hydrodynamic interaction with the obstacle. Contrary to the experimentally observed mixed motions, these trajectories are *regular*, and have a migration angle of zero, as in the case of zigzag motion. However, we still think that the computed trajectories are related to the experimentally observed mixed motions. We suppose that in the experiments the intermediate sized particles also approach the stagnation points closely, and slow down. In this position, they are prone to non-hydrodynamic interactions, like Brownian motion or colloidal forces, which could deviate them from the computed *ideal* trajectory (dividing

streamline), and make them move either above or below the obstacle. This can make the experimentally determined trajectories for mixed motion, highly irregular, and give them an intermediate migration angle in the range $0 < \theta < \theta_{\max}$.

The occurrence of three types of particle motion in the 3D simulations, namely, zigzag, displacement, and the *ideal* mixed motion, confirms that there are two critical length scales determining the particle motion. The first length scale is the width of the first flow lane, $d_{f,1}$, as postulated in our earlier classification rules. The second length scale, $d_{f,c}$, determines the occurrence of displacement motion, and appears not to be correlated with the largest flow lane width $d_{f,N}$, and is to be determined via explicit 3D particle simulations. Particles within length scales $2d_{f,1} < d_p < 2d_{f,c}$ are expected to show mixed behavior, and this is tested with the experimental results, as described in the next section.

3.2 Experimental results

The particle size (distributions) of the suspensions are illustrated in Table 3, which lists the mean particle size, $D(0.5)$, together with the $D(0.1)$ and $D(0.9)$ values, which correspond to the lower and upper 10% size limit of the particles. The experimental particle trajectories are analyzed in terms of average particle size, $D(0.5)$, and we take the $D(0.1)$ and $D(0.9)$ values as a measure for the breadth of the size distribution, which is reflected in the error bars.

Examples of particle trajectories as observed by video microscopy in ratchet design I (as listed in Table 1) are shown in Fig. 5. In Fig. 5a we present a trajectory of a particle from suspension A (see Table 3), which is showing zigzag motion. In Fig. 5b–d, we present trajectories of particles showing mixed motion, for particles from suspension D. One can clearly observe the irregularity of the mixed motion (as also observed in Kulrattanarak et al. 2010a), which starkly contrasts with the regular motion observed in the 3D simulations.

In most cases, particle adhesion has been limited or absent, as shown in Fig. 6b for suspension D flowing through design I. However, this is not always the case, and this can influence the particle trajectory considerably, as illustrated for suspension D and design II, where we

Table 3 Particle size distributions as measured in the Malvern Mastersizer 2000

Suspension	$D(0.1)$ μm	$D(0.5)$ μm	$D(0.9)$ μm
A	2.8	3.2	3.8
B	3.6	3.8	4.2
C	4.2	5.1	6.2
D	5.0	5.9	7.0

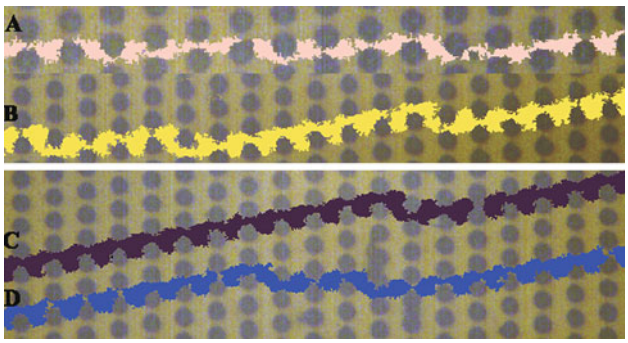

Fig. 5 Particle trajectories obtained from image analysis (Kulrattanarak et al. 2010a) in devices with $N = 4$, $R_o/D_y = 0.2$ and $D_x/D_y = 1.5$ in which **a** zigzag motion of suspension **a** occurs, and **b–d** show mixed motion of suspension **d**

observed severe particle adhesion to the obstacles (Fig. 6a). Particle adhesion is clearly a single particle event, and is probably due to colloidal forces between particles and obstacles. Despite the particle adsorption, it is still possible for particles to pass, via moving below or above the adhered particle. But adhered particles will definitely influence the local flow field and hydrodynamic interactions of particles and obstacles, and this may contribute to the irregularity of the observed mixed motion.

For each experiment, we have obtained numerous particle trajectories, which are analyzed and characterized in terms of the migration angle, which will be presented in dimensionless form, $\tilde{\theta} = \theta/\theta_{\max}$. As a measure for the distribution of the obtained migration angles, we have listed in Table 4, the number of trajectories having migration angles within a certain range. The observed trajectories are mainly obtained from the upper (upstream) half of the obstacle array, and the majority of the trajectories are of course not in the neighborhood of the confining walls, which are known to disturb the particle trajectories (Inglis 2009), making them to deviate from the "ideal" trajectories as obtained from the 3D simulations of the periodic cell.

Within the range $\tilde{\theta} < 0.1$, particles show zigzag motion, and within the range $\tilde{\theta} > 0.9$, particles show displacement motion. Particle trajectories within the other ranges are showing mixed motion. From the table we can observe that for each device the majority of the small particles show zigzag motion. With increasing particle size, the migration angles increase, but only a minority of particles show displacement motion, as aimed for in our design of the ratchet devices.

3.3 Comparison experiment with simulation

In this section, we investigate the migration angles of the particles as a function of the particle size, and compare

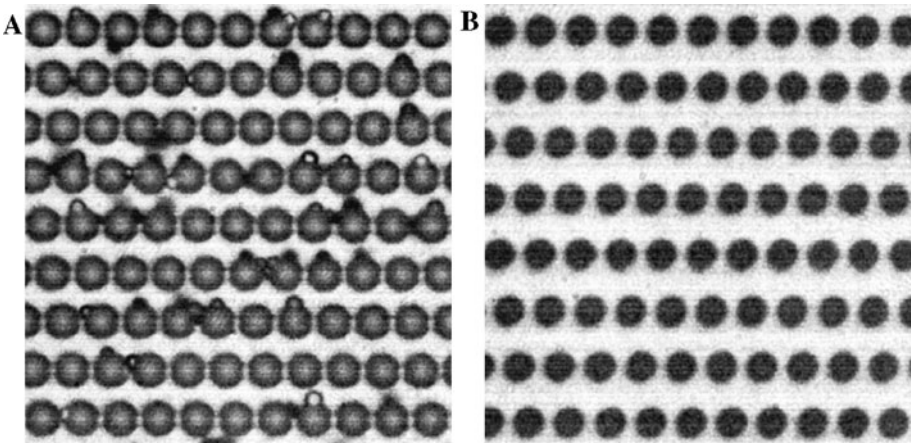

Fig. 6 Particles of suspension D (see Table 3) stuck in device design $N = 4$, $D_x/D_y = 1.5$ **a** $R_o/D_y = 0.5$ and **b** a device free of adhered particles $R_o/D_y = 0.2$

Table 4 Number of particle moving in different ranges of migration angles ($\tilde{\theta} = \theta/\theta_{\max}$)

N	R_o/D_y	D_x/D_y	$\bar{d}_p/D_y$	Number of particle trajectories			
				$\tilde{\theta} < 0.1$	$0.1 \leq \tilde{\theta} < 0.5$	$0.5 \leq \tilde{\theta} \leq 0.9$	$\tilde{\theta} > 0.9$
4	0.5	1.5	0.64^{C}	146	19	1	1
			0.74^{D}	21	5	0	1
4	0.2	1.5	0.4^{A}	145	86	0	0
			0.64^{C}	21	8	3	0
			0.74^{D}	1	8	2	1
6	0.2	1.5	0.36^{A}	354	9	1	0
			0.42^{B}	9	7	0	0
			0.56^{C}	1	8	26	5
6	0.2	2.0	0.42^{B}	219	11	0	0
			0.56^{C}	41	25	12	13
			0.65^{D}	5	10	9	15

The superscripts A–D indicate the suspensions used, as listed in Table 3

them with the numerically obtained critical length scales $d_{f,1}$ and $d_{f,c}$. The presented migration angles are the average over all migration angles, which are obtained for a particular combination of suspension and ratchet device, as indicated in Table 4. This comparison is shown in Fig. 7; the dashed lines indicate the length scales at which we expect the transitions of particle motion occur, namely, $2d_{f,1}/D_y$ and $2d_{f,c}/D_y$. Their values are directly taken from Table 2. The data points in the graphs represent the averaged, dimensionless migration angles $\theta/\theta_{\max}$, as a function of the average, dimensionless particle diameter d_p/D_y. The error bars for the particle diameter are based on the $D(0.1)/D_y$ and $D(0.9)/D_y$ values from Table 3. The error bars for the migration angle are based on the standard deviation of the migration angles, as indicated in Table 4.

Overall, the experimental results agree with the posed hypothesis for particle motion. For all particles smaller than the first lane width $r_p < d_{f,1}$, the average migration is about zero as expected. For larger particles, we find migration angles larger than zero, but smaller than unity—indicating that they are showing mixed motion as expected from the classification rules. There is one data point in Fig. 7a, which does not quite adhere to the classification rule, and in this experiment severe particle adhesion occurred, as shown in Fig. 6. Therefore, it seems legitimate to exclude this data point, and we may fairly conclude that our hypothesis on *mixed* motion is confirmed.

To investigate whether there is a correlation between migration angle and particle size, we have re-plotted all experimental data points of designs II–IV (shown in Fig. 7b–d) in a single graph, Fig. 8, displaying the normalized particle size $\tilde{d}_p = (d_p - 2d_{f,1})/(2d_{f,c} - 2d_{f,1})$ versus the dimensionless migration angle $\tilde{\theta} = \theta/\theta_{\max}$. This graph shows that $\tilde{d}_p$ versus $\tilde{\theta}$ follows a master curve. In the range of mixed motion, $0 \leq \tilde{d}_p \leq 1$, the master curve follows the straight line $\tilde{\theta} = \tilde{d}_p$. If $\tilde{d}_p < 0$ the particles are showing zigzag motion and $\tilde{\theta} = 0$, and if $\tilde{d}_p > 1$ the particles are showing displacement motion, and consequently $\tilde{\theta} = 1$.

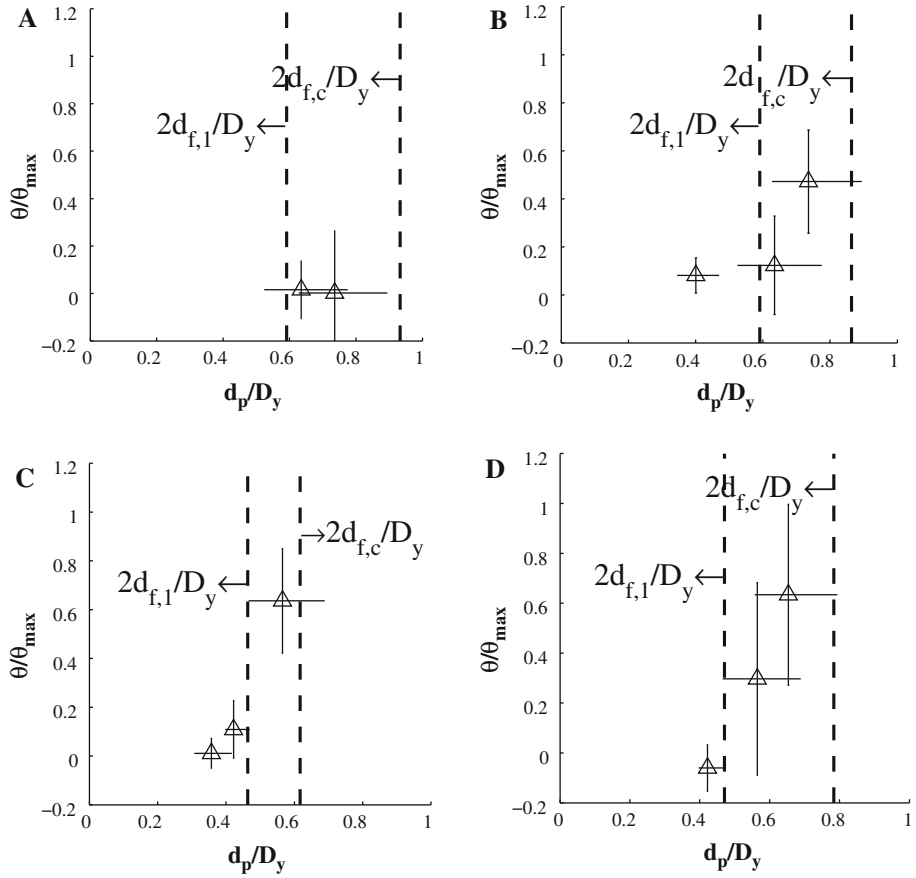

Fig. 7 Comparison of experimental results with critical length scales $2d_{f,1}/D_y$, and $2d_{f,c}/D_y$, as obtained from the numerical simulations. The experimental data are shown for ratchet designs I–IV, which are displayed in that order in graphs **a**–**d**. *Dashed lines* indicate the critical length scales, which describe (1) the transition from zigzag to mixed motion, and (2) the transition from mixed to displacement motion. Data points indicate average migration angle $\tilde{\theta} = \theta/\theta_{\max}$ versus average particle diameter d_p/D_y

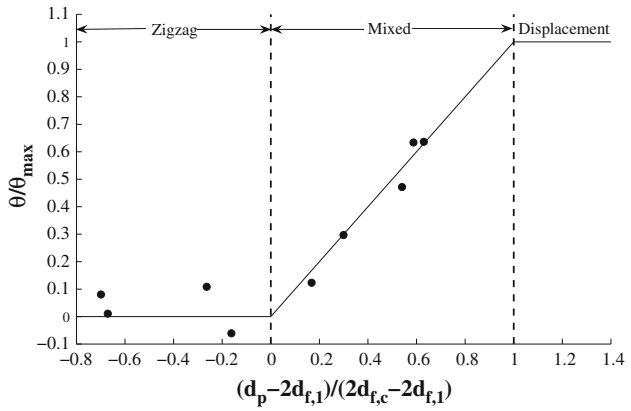

Fig. 8 An overview of migration angles obtained from the experiments compared with the length scales $d_{f,1}$ and $d_{f,c}$ obtained from 2D and 3D simulations. The *solid line* is the expected migration angle; the *dashed lines* indicate the transition points to mixed and displacement motion

4 Conclusions

In this article, we have shown experimental results that confirm our hypothesis concerning the particle motion in deterministic DLD ratchets. The particle motion is determined by 2 critical length scales: the first flow lane width $d_{f,1}$, and the second critical length scale $d_{f,c}$, which denotes the transitions to displacement motion.

The width of the first flow lane $d_{f,1}$ can be determined by simple 2D flow simulations, while the critical length scale $d_{f,c}$ needs to be determined via 3D particle flow simulations. The experimental results indicate that the migration angle θ can be determined via a set of simple rules. If $d_p < 2d_{f,1}$ then the migration angle is zero, $\theta = 0$, and if $d_p \geq 2d_{f,c}$ the migration angle is maximal, with the actual value depending on the ratchet design. For mixed motion, the migration angle follows the simple rule $\theta/\theta_{\max} = (d_p - 2d_{f,1})/(2d_{f,c} - 2d_{f,1})$.

The trajectories of particles showing mixed motion are irregular in the experiments, but the simulations show regular behavior. The numerical trajectories indicate that particles with mixed motion closely approach the stagnation points in front of the obstacles, which makes them prone to Brownian motion and/or colloidal forces, and this may influence the trajectory that is followed. In one experiment colloidal forces have been evidently at work, leading to adherence of particles.

The second critical length scale $d_{f,c}$ appears not to be correlated with any flow lane width. For now, we do not have detailed knowledge of the factors determining the size of the second critical length scale. Our previous work

Kulrattanarak et al. (2010b) indicates there is some correlation with the asymmetry of the flow lane distribution, which can be expressed in the ratio of the last to the first flow lane width: $A = d_{f,N}/d_{f,1}$. Flow lane asymmetry is induced by the symmetry breaking of the oblique primitive lattice cell used in our ratchet designs—leading to anisotropy of the permeability of the obstacle array. The relation between $d_{f,c}$, the flow lane asymmetry A and the anisotropy of the permeability of the array is clearly a good point for further investigation.

Finally, we note that the DNS simulations are performed on a single particle in the Stokes flow regime. For concentrated suspensions, relevant for food applications, there will be also hydrodynamic interactions between particles—which we expect to lead to diffusive behavior like in the case of shear-induced diffusion (van der Sman 2009; Vollebregt et al. 2010)—which may disturb the rectified motion of the displaced particles. Similar to Brownian ratchets (Keller et al. 2002), the diffusive behavior might contribute to the rectified motion if asymmetric obstacle shapes are used, like in the recent article of Loutherback et al. (2009). Food applications also call for high throughput, and consequently the flow can be beyond the Stokes flow regime. Inertia appears to change the particle behavior drastically, but enhances the selectivity of the fractionation process (Puchalla et al. 2008).

References

Adamczyk Z, Adamczyk M, van de Ven TGM. (1983) Resistance coefficient of a solid sphere approaching plane and curved boundaries. J Colloid Interface Sci 96(1):204–213

Al-Fandi M, Al-Rousan M, Jaradat MAK, Al-Ebbini L, Beech JP, Tegenfeldt JO (2010). New design for the separation of microorganisms using microfluidic deterministic lateral displacement. Robot Comput Integr Manuf. doi:10.1016/j.rcim.2010.06.003

Ball RC, Melrose JR (1995) Lubrication breakdown in hydrodynamic simulations of concentrated colloids. Adv Colloid Interface Sci 59:19–30

Brans G, Schroën CGPH, van der Sman RGM, Boom RM (2007) Transmission and fractionation of micro-sized particle suspensions. J Membr Sci 290:230–240

Chen SY, Doolen GD (1998) Lattice Boltzmann method for fluid flows. Annu Rev Fluid Mech 3:329–364

Chun B,Ladd AJC (2007) Interpolated boundary condition for lattice Boltzmann simulations of flows in narrow gaps. Phys Rev E 75(6):066705

Davis JA, Inglis DW, Morton KJ, Lawrence DA, Huang LR, Chou SY, Sturm JC, Austin RH (2006) Deterministic hydrodynamics: taking blood apart. PNAS 130:14779–14784

d'Humieres D, Ginzburg I, Krafczyk M, Lallemand P, Luo L (2002) Multiple-relaxation-time lattice Boltzmann models in three dimensions. Phil Trans R Soc Lond A 360:437–451

Eijkel JCT, van den Berg A (2006). Nanotechnology for membranes, filters and sieves. A series of mini-reviews covering new trends in fundamental and applied research, and potential applications of miniaturised technologies. Lab Chip 6:19–23

Frechette J, Drazer G (2009) Directional locking and deterministic separation. J Fluid Mech 627: 379–401

Ginzburg I (2005) Equilibrium-type and link-type lattice Boltzmann models for generic advection and anisotropic-dispersion equation. Adv Water Resour 28:1171–1195

Green JV, Radisic M, Murthy SK (2009) Deterministic lateral displacement as a means to enrich large cells for tissue engineering. Anal Chem 81(21):9178–9182

Huang LR, Cox EC, Austin RH, Sturm JC (2004) Continuous particle separation through deterministic lateral displacement. Science 304:987–990

Inamuro T, Yoshino M, Ogino F (1995) A non-slip boundary condition for lattice Boltzmann simulations. Phys Fluids 7(12): 2928–2930

Inglis DW (2009) Efficient microfluidic particle separation arrays. Appl Phys Lett 94:013510

Inglis DW, Davis JA, Austin RH, Sturm JC (2006) Critical particle size for fractionation by deterministic lateral displacement. Lab Chip 6:655–658

Inglis DW, Herman N, and Vesey G (2010). Highly accurate deterministic lateral displacement device and its application to purification of fungal spores. Biomicrofluidics 4:024109

Keller C, Marquardt F, and Bruder C (2002). Separation quality of a geometric ratchet. Phys Rev E 65:41927

Kromkamp J, Faber F, Schroën CGPH, Boom RM (2006a) Effects of particle size segregation on crossflow microfiltration performance: control mechanism for concentration polarisation and particle fractionation. J Membr Sci 268:189–197

Kromkamp J, van den Ende D, Kandhai D, van der Sman RGM, Boom RM (2006b) Lattice Boltzmann simulation of 2D and 3D non-Brownian suspensions in Couette flow. Chem Eng Sci 61(2):858–873

Kulrattanarak T, van der Sman RGM, Schroën CGPH, Boom RM (2008) Fractionation of concentrated suspensions with microfluidic devices. Adv Colloid Interface Sci 142:53–66

Kulrattanarak T, Lubbersen YS, van der Sman RGM, Schroën CGPH, Pham HTM, Sarro PM, Boom RM (2010a) Experimental observations of mixed motion in deterministic ratchets with image analysis. Meas Sci Technol (submitted)

Kulrattanarak T, van der Sman RGM, Schroën CGPH, Boom RM (2010b) Mixed motion in deterministic ratchets due to asymmetry in flow lane Distribution. J Colloid Interface Sci (in press)

Ladd AJC (1994) Numerical simulations of particulate suspensions via a discretized Boltzmann equation Part I. Theoretical foundation. J Fluid Mech 271:285–309

Ladd AJC, Verberg R (2001) Lattice-Boltzmann simulations of particle-fluid suspensions. J Stat Phys 104:1191–1251

Loutherback K, Puchalla J, Austin RH, Sturm JC (2009) Deterministic microfluidic ratchet. Phys Rev Lett 102:045301

Loutherback K, Chou KS, Newman J, Puchalla J, Austin RH, Sturm JC (2010). Improved performance of deterministic lateral displacement arrays with triangular posts. Microfluid Nanofluidics 1–7

Pham HTM, Kulrattanarak T, van der Sman RGM, Schroën CGPH, Boom RM, Sarro PM (2009) Deterministic ratchets for particle separation fabricated with Si MEMS Technology. In: Proceedings of the Eurosensors XXIII conference. Procedia Chemistry, vol 1, pp 345–348

Puchalla J, Morton K, and Austin R (2008). Velocity dependent selectivity of deterministic lateral displacement arrays. APS meeting abstracts, 9009P.

Qian YH, d'Humieres D, Lallemand P (1992) Lattice BGK model for Navier–Stokes equations. Europhys Lett 17:479–484

Sangani AS, Acrivos A (1982) Slow flow past periodic arrays of cylinders with application to heat transfer. Int J Multiphase Flow. 8(3):193–206

Steegmans MLJ, Warmerdam A, C.G.P.H. Schroen and R.M. Boom RM (2009) Dynamic interfacial tension measurements with microfluidic Y-junctions. Langmuir 25(17):9751–9758

van der Sman RGM (2009) Simulations of confined suspension flow at multiple length scales. Soft Matter 5:4376

van der Sman RGM (2010a) Confined suspension flow with MRT Lattice Boltzmann schemes. Comput Phys Commun 181(9): 1562–1569

van der Sman RGM (2010b) Effects of confinement on hydrodynamic interactions between a suspended sphere and obstacles. Phys Fluid (submitted)

Vollebregt HM, van der Sman RGM, and Boom RM (2010). Suspension flow modelling in particle migration and microfiltration. Soft Matter (in press). doi:10.1039/C0SM00217H